AD-A215 028

Solar Cycle Effects on Trapped Energetic Particles

Prepared by

A. L. VAMPOLA
Space Sciences Laboratory
Laboratory Operations
The Aerospace Corporation
El Segundo, CA 90245

15 October 1989

Prepared for

SPACE SYSTEMS DIVISION
AIR FORCE SYSTEMS COMMAND
Los Angeles Air Force Base
P.O. Box 92960
Los Angeles, CA 90009-2960

DTIC
ELECTE
NOV 24 1989
S   B   D

This report was submitted by The Aerospace Corporation, El Segundo, CA 90245, under Contract No. F04701-88-C-0089 with the Space Systems Division, P.O. Box 92960, Los Angeles, CA 90009-2960. It was reviewed and approved for The Aerospace Corporation by H. R. Rugge, Director, Space Sciences Laboratory.
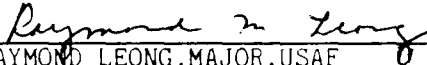
Lt Tyron Fisher was the project officer for the Mission-Oriented Investigation and Experimentation (MOIE) Program.

This report has been reviewed by the Public Affairs Office (PAS) and is releasable to the National Technical Information Service (NTIS). At NTIS, it will be available to the general public, including foreign nationals.

This technical report has been reviewed and is approved for publication. Publication of this report does not constitute Air Force approval of the report's findings or conclusions. It is published only for the exchange and stimulation of ideas.

TYRON FISHER, LT, USAF
MOIE Project Officer
SSD/CLFPL

RAYMOND LEONG, MAJOR, USAF
MOIE Program Manager
AFSTC/WCO

REPORT DOCUMENTATION PAGE

1a. REPORT SECURITY CLASSIFICATION Unclassified	1b. RESTRICTIVE MARKINGS
2a. SECURITY CLASSIFICATION AUTHORITY	3. DISTRIBUTION/AVAILABILITY OF REPORT Approved for public release; distribution unlimited.
2b. DECLASSIFICATION/DOWNGRADING SCHEDULE	

4. PERFORMING ORGANIZATION REPORT NUMBER(S) TR-0089(4940-05)-3	5. MONITORING ORGANIZATION REPORT NUMBER(S) SD-TR-89-78

6a. NAME OF PERFORMING ORGANIZATION The Aerospace Corporation Laboratory Operations	6b. OFFICE SYMBOL (If applicable)	7a. NAME OF MONITORING ORGANIZATION Space Systems Division
6c. ADDRESS (City, State, and ZIP Code) El Segundo, CA 90245		7b. ADDRESS (City, State, and ZIP Code) Los Angeles Air Force Base Los Angeles, CA 90009-2960

8a. NAME OF FUNDING/SPONSORING ORGANIZATION	8b. OFFICE SYMBOL (If applicable)	9. PROCUREMENT INSTRUMENT IDENTIFICATION NUMBER F04701-88-C-0089

8c. ADDRESS (City, State, and ZIP Code)	10. SOURCE OF FUNDING NUMBERS			
	PROGRAM ELEMENT NO.	PROJECT NO.	TASK NO.	WORK UNIT ACCESSION NO.

11. TITLE (Include Security Classification)

SOLAR CYCLE EFFECTS ON TRAPPED ENERGETIC PARTICLES

12. PERSONAL AUTHOR(S)

Vampola, Alfred L.

13a. TYPE OF REPORT	13b. TIME COVERED FROM _____ TO _____	14. DATE OF REPORT (Year, Month, Day) 15 October 1989	15. PAGE COUNT 44

16. SUPPLEMENTARY NOTATION.

17. COSATI CODES			18. SUBJECT TERMS (Continue on reverse if necessary and identify by block number)
FIELD	GROUP	SUB-GROUP	Magnetospheric Particles Solar Cycle Effects Space Environment

19. ABSTRACT (Continue on reverse if necessary and identify by block number)

The energetic particle populations in the earth's magnetosphere, which are the result of geomagnetic activity and, ultimately, are due to solar activity, have a major impact on the operation and survival of spacecraft. Departures from the nominal in solar activity produce requirements for changes from the nominal in the design and operation of spacecraft. If the approaching solar maximum is a robust one, as is indicated by preliminary solar data, the energetic particle population can be expected to be in excess of that predicted by particle models such as AE8 and AP8, since those models include solar cycle effects based on nominal solar activity. In the event of a robust solar cycle, accelerated degradation of electronics and power systems, increased sensor background effects, and more frequent operational anomalies may be expected on spacecraft which were designed for a nominal solar cycle. This report discusses the relationships between solar activity and geomagnetic activity and provides a short tutorial on the mechanisms by which the energetic particle environment is produced and modified by magnetic activity. As an aid to spacecraft systems design and mission planning, the report also indicates the types of changes from a nominal energetic particle population that could be expected based on a robust solar Cycle 22.

20. DISTRIBUTION/AVAILABILITY OF ABSTRACT ☐ UNCLASSIFIED/UNLIMITED ☒ SAME AS RPT ☐ DTIC USERS	21. ABSTRACT SECURITY CLASSIFICATION Unclassified
22a. NAME OF RESPONSIBLE INDIVIDUAL	22b. TELEPHONE (Include Area Code) 22c. OFFICE SYMBOL

DD FORM 1473, 84 MAR   83 APR edition may be used until exhausted   SECURITY CLASSIFICATION OF THIS PAGE
All other editions are obsolete

UNCLASSIFIED

CONTENTS

FIGURES

I. INTRODUCTION

Thus far, the sunspot numbers and the $F_{10.7}$ index for Cycle 22 are much larger than and rising at a faster rate than had been predicted on the basis of past solar cycles. In recent history, the sunspot maximum has been alternating between a moderate maximum and a small maximum. Cycle 19 was large, Cycle 20 was small, and Cycle 21 was intermediate between the previous two cycles. Cycle 22 was generally predicted to be small. The latest data (2/89), however, now indicate that Cycle 22 will be more like Cycle 19.

The first data which were used for modeling the trapped radiation in space date from 1964, which was during the minimum between Cycles 19 and 20. More recent models are based on a short data period in 1968. Thus, we have no measurements of energetic trapped particles in space during a "robust" solar cycle. It is appropriate, therefore, to make estimates of what the trapped particle environment will be in the event of a solar cycle similar to Cycle 19.

The energetic particle populations trapped in the earth's magnetosphere provide a very hostile environment for space systems. Spacecraft missions are heavily impacted by the trapped energetic particle environment in a number of ways. At high altitude, electrical charging of spacecraft surfaces, which occurs as a result of hot plasma ($E_e \sim 20$ keV) injected from the geomagnetic tail during magnetic substorms, can produce surface discharges which result in spurious operation of or damage to the spacecraft. Energetic electrons (~0.5 to 1.5 MeV) embed within dielectrics, producing potentials in excess of the breakdown potential of the material, again resulting in discharges which act as spurious signals or can damage sensitive components. Radiation dose effects, which are observed at all altitudes, limit the operational life of sensitive microcircuits, electronic systems, and solar cells.

At a lower level of effect, basically a nuisance level, energetic protons and electrons produce spurious signals and backgrounds in detection systems of various types, including their optics and sensors. At the lowest disturbance threshold, particle-induced backgrounds present complications in the form of increased dead-time and/or requirements for increased signal processing. Energetic particles, through the deposition of energy in matter, can produce spurious signals on any sensor, *e.g.*, Cerenkov radiation in optical sensors; photocathode noise in photomultipliers; direct energy deposits in solid state detectors, whether they be silicon CCD arrays, HgCdTe infrared (IR) sensors, or other types of systems. In each of these situations, the energy deposit mimics the expected signals or increases the background, thereby reducing the sensitivity of the system, increasing the dead-time of the sensor, or causing an increase in the signal processing complexity.

At the next level of energetic particle environmental effects on space systems, two additional mechanisms become important. The first is direct thermal input to low temperature systems, especially those with passive radiators designed to operate at temperatures under 100 K. In some orbits, the transient energy input[1] due to the energetic particle population can exceed 5 W/m^2. For ultra-low temperature IR sensors, such as on the InfraRed Astronomy Satellite (IRAS), this additional heat load must be considered in the design of the thermal management system and could be a major element in the design. Moderate and major magnetic storms produce large increases in the energetic particle population (orders of magnitude) that can increase the heat load *averaged* over an orbit by an order of magnitude. These large increases in heat input may persist for several days.

The second low level effect--the direct deposition of charge by electrons which stop in thick dielectrics, which was mentioned briefly previously--occurs when the flux of 0.5 to 1.5 MeV electrons is sufficiently high. At times, this effect produces electric fields in excess of the breakdown potential of the dielectric.[2] The subsequent discharge can act as a spurious signal (such as a control signal in a coaxial cable) or can damage sensitive components which are connected to the cable in which the discharge occurs. It has been estimated that in geosynchronous orbits, as high as 50% of the electrostatic discharge anomalies are due to this thick dielectric charging mechanism.[3]

While the disruptions due to spacecraft charging may have a major impact on a satellite mission, including terminating it,[4] the charging problems are not ubiquitous. Many orbits, especially low altitude ones, are not concerned with this mechanism. Virtually all satellites, however, are designed to radiation dose and dose-rate specifications. The radiation damage to solar cells, for example, is a major parameter in the design of satellite power systems. Satellites which are designed for long missions in the heart of the outer zone, such as the Global Positioning System vehicles, are constructed with specially designed radiation-hardened devices. Since the cost of a radiation-hardened microchip is much greater than its non-hardened equivalent, a good estimate of the expected radiation environment is required in order to ensure that rad-hard devices are used when and where needed and not elsewhere. Furthermore, proper estimates are necessary to assure adequate design and test levels. Thus, space system designers require long-range predictions of the energetic particle environment. Solar activity--via an increased solar wind momentum and changing magnetic vector which couple into the earth's magnetosphere--produces the magnetic storms and substorms which accelerate charged particles in the magnetosphere. Since the energetic particle population is a direct result of solar activity, this translates into a need for long-range predictions of solar activity. Since the predictions for system designers are usually given in the form of long-term averages or long-term trends of magnetospheric particle populations (models), a significant departure in the solar activity cycle from that which was

6

expected could have a major impact on both the design of satellites due to be in orbit during the coming solar maximum and on the operation of satellites which were not designed to accommodate a larger-than-normal solar activity cycle.

Since solar activity has a direct impact on the energetic particle population, we will discuss the mechanism by which the sun produces geomagnetic disturbances which modify the energetic particle environment. We will present data showing the effect of magnetic perturbations on the magnetospheric particle populations. We will discuss a number of areas of satellite operations in which particle flux increases have an impact on the mission; then we will discuss briefly the deviations from the energetic particle environment models that can be expected for a robust solar cycle.

II. SOLAR ACTIVITY–MAGNETOSPHERIC PARTICLE RELATIONSHIP

The ultimate source of all of the energy of the magnetospherically trapped particle population is the sun. In the absence of the solar wind, the earth's geomagnetic field would be quiescent and, in the near-earth region, would be roughly symmetrical about the magnetic axis. It would extend outward to large distances. In the presence of the solar wind, however, the geomagnetic field is grossly distorted. On the sub-solar side, the magnetosphere terminates at a location, termed the magnetopause, determined by the properties of the solar wind. During moderate solar wind conditions, the magnetopause is typically at about 10 earth-radii altitude, as depicted in Fig. 1.

The solar wind, a plasma flow, consists primarily of ionized hydrogen and helium plus associated electrons which produce an electrically neutral ensemble. Typical densities are of the order of $10/cm^3$, and typical velocities are of the order of 350 km/sec. Both of these parameters may vary by a factor of 2 (greater or smaller) on a short time scale. The magnetic field present in the region of the sun where the plasma originated is "frozen" into the plasma flow because the energy density of the plasma exceeds that of the magnetic field. This plasma flow comprises a significant energy and momentum density. The solar wind, being composed of charged particles, cannot penetrate deeply into the geomagnetic field. The plasma, with its embedded solar magnetic field, compresses the geomagnetic field until pressure balance is achieved: the magnetic pressure of the earth's field equals the momentum pressure of the solar wind. Discussion of the actual mechanism of this pressure transfer, involving a collisionless shock ("Bow Shock" in Fig. 1), is beyond the scope of this presentation.

Changes in the orientation of the embedded solar magnetic field (the interplanetary field depicted in Fig. 1), the solar wind density, or the solar wind velocity all cause perturbations in the geomagnetic field. The orientation of the interplanetary magnetic field is a major factor in the coupling of solar wind energy into the geomagnetic field.[5] The solar wind flows around the flanks of the magnetosphere and, through the production of surface currents which flow at the magnetopause and produce a viscous interaction, stretches the geomagnetic field into a long tail, up to perhaps 300 earth-radii. At some point downstream, the tail field lines are not closed; they connect to the solar magnetic field embedded in the solar wind (Fig. 1). Obviously, a change in polarity of the embedded field produces a drastic change in the configuration of the geomagnetic field. A magnetic storm or substorm occurs.

Within the tail, plasma (originating either in the ionosphere or in the solar wind) is heated by the viscous flow mentioned above. The heating increases the internal pressure, which
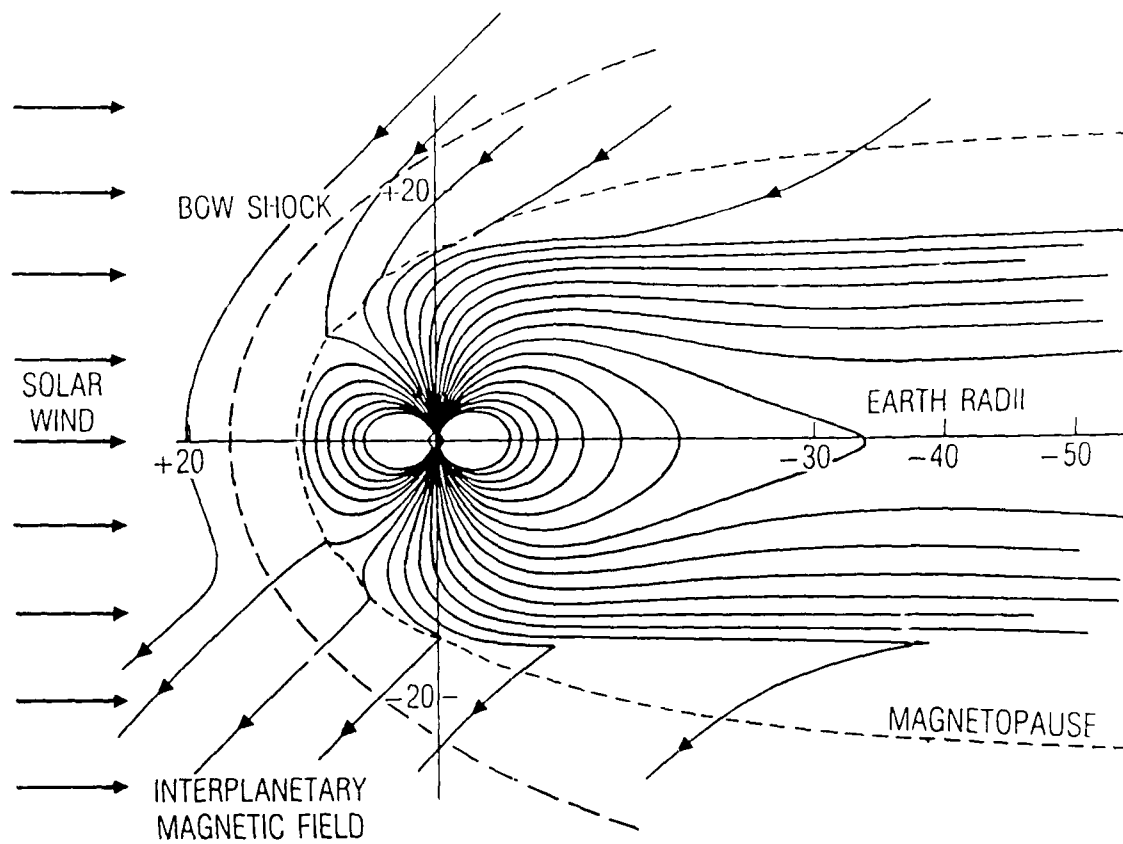
9

Fig. 1. Solar Wind-Geomagnetosphere Interaction Geometry

stretches the tail field lines further. Then, either through a disruption of the tail field lines ("the far end of the tail separates") or by exceeding the pressure which can be sustained by the tail field lines, heated plasma is ejected earthward, and a substorm occurs. (The only difference in these two views of substorm dynamics is the question of whether plasma and magnetic field, which were once part of the tail, separate and move downstream with the solar wind. In both cases, plasma is heated and injected into the inner magnetosphere.) The substorm signature is observed on ground-based magnetometers (utilized in deriving the magnetic index K_p, a planetary high latitude index).

When a very substantial change occurs in the interplanetary medium, such as a large increase in solar wind density due to a solar flare or a large increase in solar wind velocity due to a coronal hole, major modifications of the geomagnetic configuration occur. Coronal holes are regions on the sun where the plasma pressures are sufficiently high that the pressure overcomes the magnetic field containment. The resulting flow of plasma cools the region, producing a lower temperature area, which appears darker than the surrounding area. Coronal holes, which can persist over a number of solar rotations,[6] and which are more prevalent during the declining phase of the cycle, are sources of high speed wind streams. When the high speed wind stream impacts the magnetosphere, the plasmapause may be pushed substantially earthward, even to a location within the geosynchronous orbit. The whole configuration may be displaced, with the auroral oval moving to higher latitudes on the day side and to lower latitudes on the night side. These changes in the magnetospheric configuration are accompanied by changes in the high latitude ionospheric current system (the auroral electrojet) and sometimes by the injection/acceleration of energetic ions deep within the magnetosphere. These ions, called the *ring current*, produce a diamagnetic effect equivalent to a current circling the equator at high altitude, which reduces the geomagnetic field. The magnetic index D_{st}, which is an average of the reduction of the horizontal component of the magnetic field as measured at a number of low latitude stations around the world, is a measure of this ring current. D_{st} is expressed in units of gammas or nanoteslas. We will discuss the effects of all of this magnetic activity on the energetic particles in the earth's magnetosphere later.

In summary, variations in the solar wind produce magnetic activity which is measurable on the ground and is related to changes in the plasma and energetic particle population in the magnetosphere. The relationship between the solar cycle and D_{st} is shown in Fig. 2. In this figure, the lower panel depicts the monthly mean sunspot numbers for the time period 1957-1984, which covers the last half of Cycle 19 plus all of Cycles 20 and 21. The smoothed numbers which are usually quoted are derived from the monthly mean numbers. The upper panel presents the daily mean of D_{st} for the same time period. The correlation between the daily mean of D_{st} and the smoothed sunspot numbers is readily observable. It has been noted in the past that solar flares

Fig. 2. Comparison of Monthly Mean Sunspot Numbers and Daily Mean D_{st} for 1957 to 1984

and energetic particle events in the geomagnetic field tend to show an increase during the rising part of the sunspot cycle, a relative reduction at the peak of the sunspot cycle, and another increase in activity during the first couple of years of the declining phase. The D_{st} data in Fig. 2 appear to show the same feature. With the exception of one very active month during 1967 (and ignoring the lack of a pronounced peak in D_{st} at the time of the peak in sunspots), the D_{st} plot, in fact, appears to correlate very well with the solar sunspot cycle. Both the number of large (negative) values of D_{st} and the maximum observed values of D_{st} correlate with the sunspot cycles. During Cycle 20, which peaked in 1969, both the number of sunspots and the excursions in D_{st} were less than in the other two cycles. It would appear that if the present cycle is going to be a major one, perhaps similar to Cycle 19, D_{st} will show major activity also. As will be shown, large negative D_{st} correlates with high energetic particle fluxes in the magnetosphere.

III. TRAPPED PARTICLE MORPHOLOGY

In the preceding section, we have seen that geomagnetic activity, as evidenced in the magnetic index D_{st}, is correlated with the sunspot cycle (with the exception of a minor reduction in D_{st} excursions right at the sunspot maximum). In the next section, we will demonstrate the correlation between magnetic activity and the trapped energetic particle populations. But to understand how magnetic storms can affect the particle population, we will first discuss how magnetic fluctuations affect individual charged particles.

In this section, three subjects will be discussed: trapped particle motions, how the solar magnetic field interacts with them, and McIlwain's "L" parameter. The discussion is at an introductory level; no previous knowledge about the particle radiation environment is assumed. The intent is to provide sufficient background material about radiation belt morphology so that the rest of this presentation and the other papers in the Solar Cycle Effects group which deal with particle radiation effects will be understood in context. Those who are knowledgeable about radiation belt morphology can skip forward to the next section.

A. TRAPPED PARTICLE MOTIONS

An understanding of the effects of solar activity on the trapped radiation population requires a knowledge of the dynamics of the radiation belts. This, in turn, requires some knowledge of the dynamics of an individual particle. We will briefly discuss these dynamics. The three basic particle motions in the earth's magnetosphere with which we are concerned are gyration or cyclotron motion, bounce, and drift. The gyration is about the local magnetic field line, the bounce motion is from one end of the field line to the other (one hemisphere to the other), and the drift is around the world in longitude. These motions are a consequence of the behavior of a charged particle with forces acting on it moving in a non-uniform magnetic field. To the extent that solar activity produces measurable changes in the geomagnetic field, such as magnetic storms, this solar activity also modifies the motion of the trapped particles and their characteristics. Thus, an understanding of the basic motion of the particles is necessary to an understanding of how solar activity affects the trapped particle population. To produce a permanent change in the properties of the particle distribution, the time scale of the changes in the magnetic field have to be on the order of or shorter than one of the characteristic periods of motion of the particle.

In a uniform magnetic field B, a charged particle q moving with velocity v experiences a force which appears as an electric field E at right angles to both the direction of the field B and the

component of the velocity vector perpendicular to that field ($E = -q \, v \times B$ in vector notation, where the boldface denotes a vector). Since, at each instant, this electric field tends to change the direction of the particle, which, in turn, changes the direction of the effective electric field, the particle executes a circular path--it gyrates about the field. This coupling of forces also results in a complementary behavior: imposition of force upon a charged particle initially at rest in a magnetic field results in motion in a net direction perpendicular to both the force and the magnetic field (components of force along the field and curvature of the field are ignored here). The three basic motions of trapped particles in the magnetic field are a consequence of these force couplings and of the fact that the geomagnetic field has curvature and intensity gradients. Because of the curvature and intensity gradients, the particle's gyration path does not close upon itself, resulting in a drift motion. The motions are shown in Fig. 3.

The direction of gyration follows the *right hand rule* for both electrons and ions; since the charges are opposite for the two types of particles, the direction of gyration is opposite for the electrons and ions, and therefore the direction of drift is also opposite, with electrons and negative ions drifting eastward and protons and other positive ions drifting westward. The frequency of gyration, called the *Larmor frequency*, is given by:

$$f_L = \Omega_1 / 2\pi = -q \, B / 2\pi \, m_0 \, \gamma \, c \qquad (1)$$

Note that since the frequency of gyration is proportional to B, it is not constant along the field line. It is a minimum at the magnetic equator and increases as the particle moves away from the equator. For non-relativistic particles ($\gamma \approx 1$), the frequency of gyration is also independent of energy. Typical equatorial frequencies at 1000 km altitude are around 0.5 MHz for very low energy electrons and about 300 Hz for low energy protons. High energy particles have lower gyrofrequencies because of their greater (relativistic) mass. In the following discussion, we will ignore the energy loss which results whenever a charge is accelerated (called *Bremsstrahlung* when it occurs in the electrostatic field of a nucleus and *betatron radiation* when it is produced by a magnetic field) because the energy loss is very small for particles trapped in the geomagnetic field.

B. THE FIRST ADIABATIC INVARIANT

If one analyzes the path of a particle gyrating in a magnetic field, one observes that it encloses a fixed amount of flux which depends on the momentum of the particle perpendicular to the magnetic field. Under static conditions, the flux can't "leak" out of the path. This flux quantity, which is the origin of the magnetic moment of the particle, is *invariant* as long as conditions are adiabatic; *i.e.*, the magnetic field is quiescent and no energy is added to the particle.
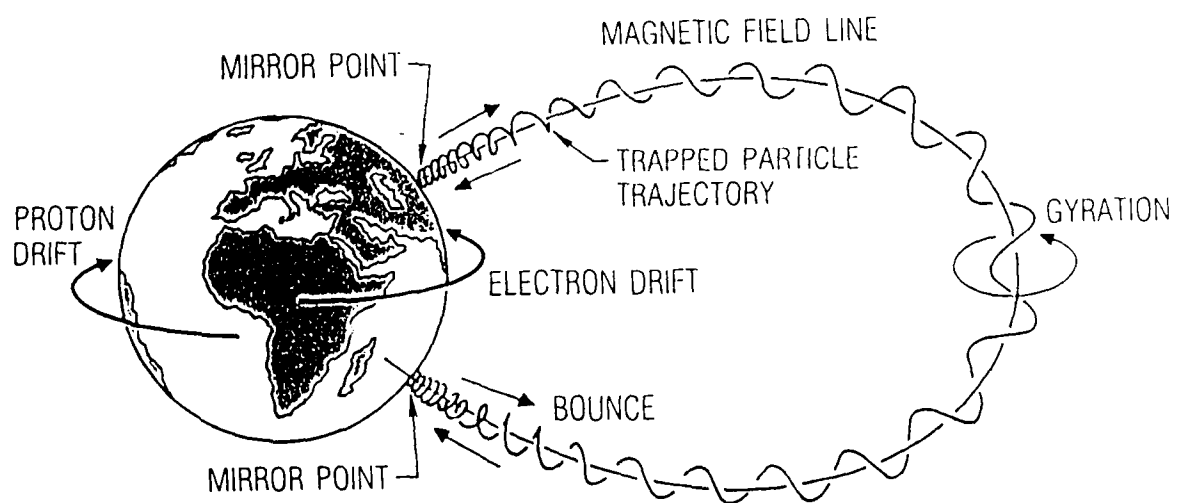
16

Fig. 3. Geomagnetically Trapped Particle Motions

It is called the *first adiabatic invariant*, usually denoted by M ($=p_\perp^2/2m_0B$). The radius of gyration, ρ ($=mv/Bq$), is inversely proportional to B. Thus, the total flux enclosed by the path (flux density times area) is inversely proportional to the *square* of the magnetic field. But, if the magnetic field increases by an amount ΔB, thereby decreasing the radius of gyration, the perpendicular momentum of the particle has to increase to conserve the magnetic moment--to maintain the total flux enclosed by the path constant. Otherwise, the area of flux enclosed by the gyration path would have decreased by ΔB^2, while the flux density increased by only ΔB. This has two interesting consequences.

First, it produces the bounce motion of particles in the geomagnetic field. A particle starting out at the equator with a component of velocity along the field line will travel a helical path to lower altitude with the field line as a guiding center. As the particle moves, it is moving in an increasing field. In order to maintain a constant magnetic moment, the momentum component perpendicular to the magnetic field has to increase. In the absence of such an increase, the magnetic moment would be decreasing as 1/B. The only sources of energy available to provide this perpendicular momentum increase are the magnetic field and the particle kinetic energy. In a quiescent field, all of the perpendicular momentum increase is obtained from the particle motion by converting momentum parallel to the field into momentum perpendicular to the field. When this source is exhausted, the particle motion parallel to the field line is zero and the particle is gyrating at a field intensity B_m, called the *mirror B*. The gradient in the field then reverses the process (called *mirroring*), and the particle travels a helical path to the other hemisphere, where it again mirrors at a magnetic field intensity B_m exactly equal to the previous one. The two mirror points are called *conjugate* points because they are *joined* by the field line, which is the guiding center of this helical motion. The particle actually spends most of its time at these mirror points.

The second interesting consequence which follows from conservation of the first adiabatic invariant is acceleration of the particle by an increasing magnetic field (*e.g.*, that due to a compression of the geomagnetic field by an increase in the momentum density of the solar wind). As noted above, the only sources of energy to maintain a constant magnetic moment in an increasing field are the particle motion and the field itself. If the field is changing, the particle may maintain its magnetic moment by increasing its perpendicular momentum at the expense of the magnetic field. This is, in fact, the source of the energy contained in the trapped energetic particle populations. Consider a particle that is mirroring so that all of its momentum is perpendicular momentum. If the field then increases, the field must accelerate the particle to increase the particle's perpendicular momentum (which must be done to conserve the total flux enclosed within the particle's gyration path). Note that the particle still has the same magnetic moment after it has been accelerated as it had previously; it has a smaller radius of gyration, but it is now at a higher energy. The reverse process also works: a decreasing field will decelerate particles. Geomagnetic

activity does both, producing radial displacements in the process. If the third adiabatic invariant, discussed below, is violated, the result is radial diffusion (a process in which particles initially on the same field line are transported to higher and lower field lines), which results in a net increase of energetic particles in the outer zone. These energetic particles then diffuse both inward and outward.

C. THE SECOND ADIABATIC INVARIANT

The bounce motion described above also has an associated invariant, called the *second adiabatic invariant*. Basically, it is the total magnetic field energy contained within the envelope of the helical path between mirror points. (This function, like the other invariants, can be evaluated as a line integral. The details are beyond the scope of this discussion.) Note that if the magnetic field is increased, the energy density is increased. The radius of gyration is reduced to compensate (first invariant, described above), but the path length must also be reduced. Thus, the mirror points must be raised. Conversely, if the field weakens, mirror points can also be lowered and the particles could be lost into the atmosphere. The bounce period is only a weak function of the equatorial pitch angle of the particle (the angle between the particle velocity and the magnetic field line at the magnetic equator), since the particles spend most of their time at the mirror points. The bounce period can be approximated by:[7]

$$2\pi/\Omega_2 = (4 L R_e / v) T(y) \tag{2}$$

where T(y) is given by:

$$T(y)=1.3802-.31985(y+y^{1/2})$$

Representative bounce periods for 1 MeV electrons and protons at 1000 km altitude are 0.1 and 1 sec, respectively. From Eq. (2), it is seen that the bounce period is proportional to energy and inversely proportional to L.

D. THE THIRD ADIABATIC INVARIANT

Because the field has a radial gradient and curvature, the radius of curvature of the gyration or orbit about the field line is larger at the top of the orbit than at the bottom (top and bottom referenced with respect to the earth radial direction). Thus, the path does not quite close into a circle, and the next orbit starts slightly eastward (for electrons) or slightly westward (for positive ions) from the previous gyration. This advance in position results in a drift motion

19

around the earth. After one drift period around the earth, the particle will be back at the same location in the field where it started, provided the field is quiescent. The locus of points through which the particle passes is called its *drift shell*. The total flux enclosed by this shell is also a conserved quantity. It is the conservation of this flux function, or *third adiabatic invariant*, that causes the particle drift shell to close after one drift period. However, during the time required for a particle to drift around the earth, the magnetic field itself may change. During large magnetic storms, the change can be quite substantial, up to 1%. After one drift period, the particle may find itself on a different drift shell with a different field intensity (and therefore a different energy). The resulting violation of the third adiabatic invariant is the primary source of particle acceleration in the magnetosphere.

The drift period is a function of the bounce period [note that the T(y) in Eq. (2) shows up in Eq. (3)] and can be approximately represented by:[7]

$$2\pi/\Omega_3 = -(3L/2\pi\gamma)(\gamma^2-1)(c/R_e)^2(m_0/qB_0)D(y)/T(y) \qquad (3)$$

where D(y) is given by:

$$D(y) = \frac{1}{12}[5.5208-0.4381y-0.6397(y \ln y + y^{1/2})]$$

Representative drift periods for 1 MeV electrons and protons at 1000 km altitude are about 1 hr and a half-hour, respectively. From Eq. (3), it is seen that the drift period is also proportional to energy and inversely proportional to L.

E. McILWAIN'S L PARAMETER

As a result of conservation of the first invariant, a particle's instantaneous pitch angle as it moves along a field line can be expressed in the form:

$$\mathrm{Sin}^2\,\alpha_i\,/\,B_i = \mathrm{constant} \qquad (4)$$

As a consequence of this relationship between B and α, if one knows the pitch angle of a particle at any point on the field line between the mirror points, one also knows B_m (which is the point at which $\alpha = 90°$). The loci of these mirror points as the particle drifts around the earth are two rings of constant B_m (one in each hemisphere). Provided one knows the unidirectional flux all along the field line below a point, the relationship expressed by the above equation permits the conversion of unidirectional fluxes to omnidirectional fluxes along the same region of the field line. In a similar manner, one can reconstruct the unidirectional flux from the omnidirectional

20

flux. However, in practice, it is much easier to measure the unidirectional flux along the field line (which can be done from a single equatorial point by using an instrument that scans in the angle α) than to measure the omnidirectional flux distribution (which would have to be done by making measurements at closely spaced points all along the field line).

As a particle drifts around the earth, the conservation of the second invariant results in the particle's guiding center tracing out a shell which connects the two rings of mirror points. The third invariant produces the result that the shell is closed upon itself--a particle remains on the same shell as it drifts around the earth. Of course, if the magnetic field varies during a drift period (or bounce or gyration period), the adiabat associated with that motion will no longer be precisely conserved. As previously stated, such violation of conservation due to magnetic field fluctuations results in pitch angle diffusion, cross-field particle diffusion, and in changes in the energy of the particles.

Mapping of the particle population in the magnetosphere requires multi-dimensional labeling: particle species; energy; pitch angle; and altitude, latitude, and longitude. The task of mapping the radiation environment is greatly simplified by reducing the three spatial coordinates to two magnetic coordinates, B and L, which are essentially the drift shells (L) and rings of constant B (an example being B_m, described above). The adiabatic invariant associated with the bounce motion, I, is obtained by integrating the function $(1-B/B_m)^{1/2}$ between the mirror points. Since this is awkward to do in the distorted geomagnetic field (the field has to be represented by a multipole expansion), an approximate relation is derived which can be related to a dipole field: L^3 $B / M_e = F(I^3 B / M_e)$. Here M_e is the dipole moment of the geomagnetic field. The function F can be calculated at a number of points, generating an interpolation table. L then becomes a simple calculation.[8] Note that for the real magnetic field, L is only an approximate representation of I, although a sufficiently accurate representation for mapping purposes. For a dipole, $L = R_0$, where R_0 is the normalized distance from the center of the dipole to the equatorial crossing of the field line labeled "L". For our purposes, the dipole approximation will provide some understanding without belaboring the mathematics:

$$R = L \cos^2 \lambda \qquad (5)$$

$$B = M/R^3 (4 - 3 R / L)^{1/2} \qquad (6)$$

where R and λ are the usual radial distance and magnetic latitude in a dipole field, M is the dipole moment, and L is McIlwain's parameter. Note that R and λ are not sufficient to describe the spatial characteristics of the particle distributions, since a given particle does not drift at a constant R or mirror at a constant λ except in a true dipole field where the azimuthal symmetry produces a

degeneracy. The above expression shows that in a dipole field, L would correspond to the radial distance from the center of the earth to the equatorial crossing of the magnetic field ($\lambda = 0°$).

IV. CORRELATION OF MAGNETIC ACTIVITY WITH ENERGETIC PARTICLE FLUXES

After that considerable digression, we are ready to discuss the effects of geomagnetic activity, and therefore solar activity, on the geomagnetically trapped energetic particle populations. We will discuss these effects as a function of particle species (electrons and protons) and altitude, but first we shall demonstrate that geomagnetic activity is highly correlated with the energetic electron population in the magnetosphere. For use in the following discussions, the terms *inner zone* and *outer zone* will be used to define the L<2.4 and L>2.4 regions of the magnetosphere, in accordance with the division of the NASA particle environment models into inner and outer zones.

The very energetic electron environment at high altitudes is intimately controlled by geomagnetic activity. Figure 4 shows the effect of a major magnetic storm on energetic electrons in the outer zone.[9] In this case, the storm (D_{st}=-145 nanotesla) occurred on 15 May 1969. Fluxes of electrons with energies above 1 MeV in the outer zone are seen to increase by 2 orders of magnitude over the pre-storm levels. At 200 keV, the increase is about 3 orders of magnitude. Note that the most energetic electrons, those with energies above 1 MeV, take the longest to decay away. For the event of Fig. 4, electron fluxes above 2 MeV peak two weeks after the storm and are just beginning to decay at 3 weeks after the storm. Increases such as these show up in satellite operations as increased anomaly rates due to thick dielectric discharges, increased heating of cryogenic radiators in some orbits, and increased background levels in sensors. Electronic devices that are near their tolerance limit for radiation damage also have a much higher probability of failure during one of these large particle increases.

Statistical approaches also demonstrate the relationship between magnetic activity and the energetic particles. In Fig. 5, the correlation between D_{st} and energetic electrons trapped in the geomagnetic field is shown for a period of almost a year. The middle and upper panels are the daily averages of electron flux at 0.5 and 2.5 MeV for a number of L-shells during 1969. Note that logarithmic flux scales are used. The particle data were all obtained by the OV1-19 satellite at about 5000 km altitude.[10] It has been shown previously[11] that the low altitude flux comes into equilibrium with the equatorial flux within 0.1 days after a major particle injection/acceleration event. Thus, the data of Fig. 5, being daily averages, are representative of the total flux trapped on those field lines even though these data were obtained at relatively low altitude. Fluxes higher on the field line are higher. The bottom trace is the daily mean D_{st} for the same time period. Note that all major excursions of D_{st} are well correlated with major excursions in the 0.5 MeV particle population at L=3.5 (lower panel). This location is essentially the heart of the outer zone during average conditions. The higher L-shells, 4.5 and 5.5, respond to additional smaller excursions in
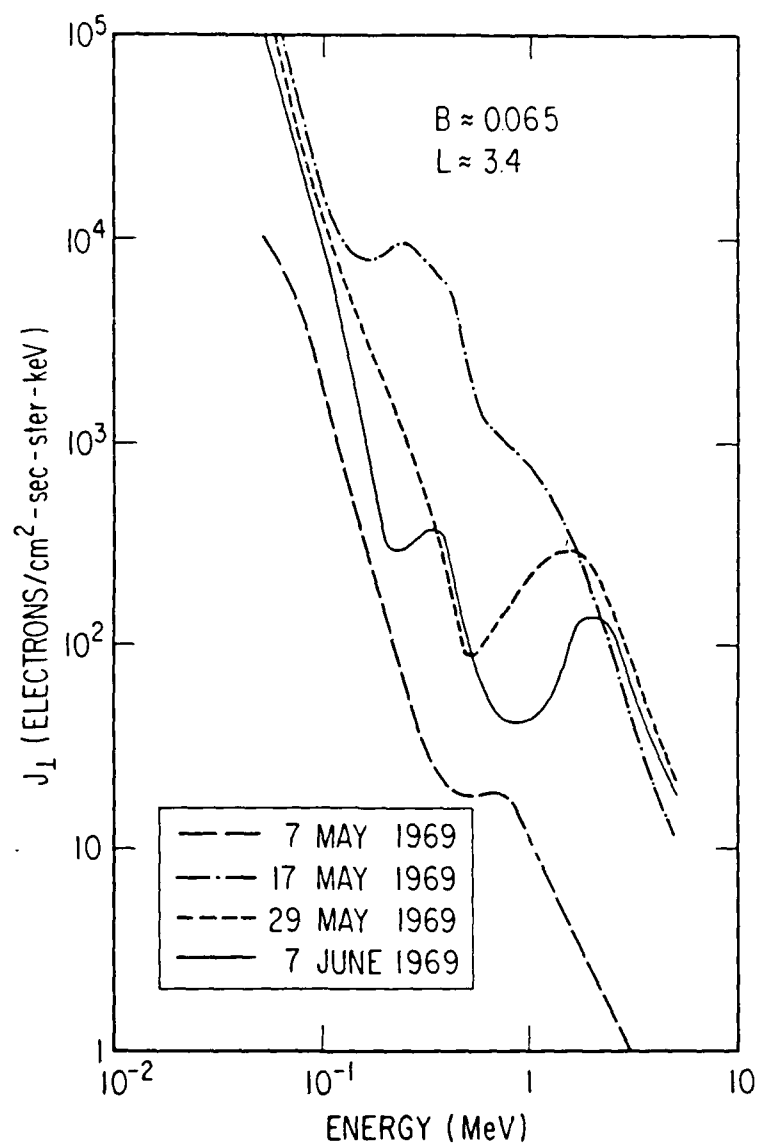
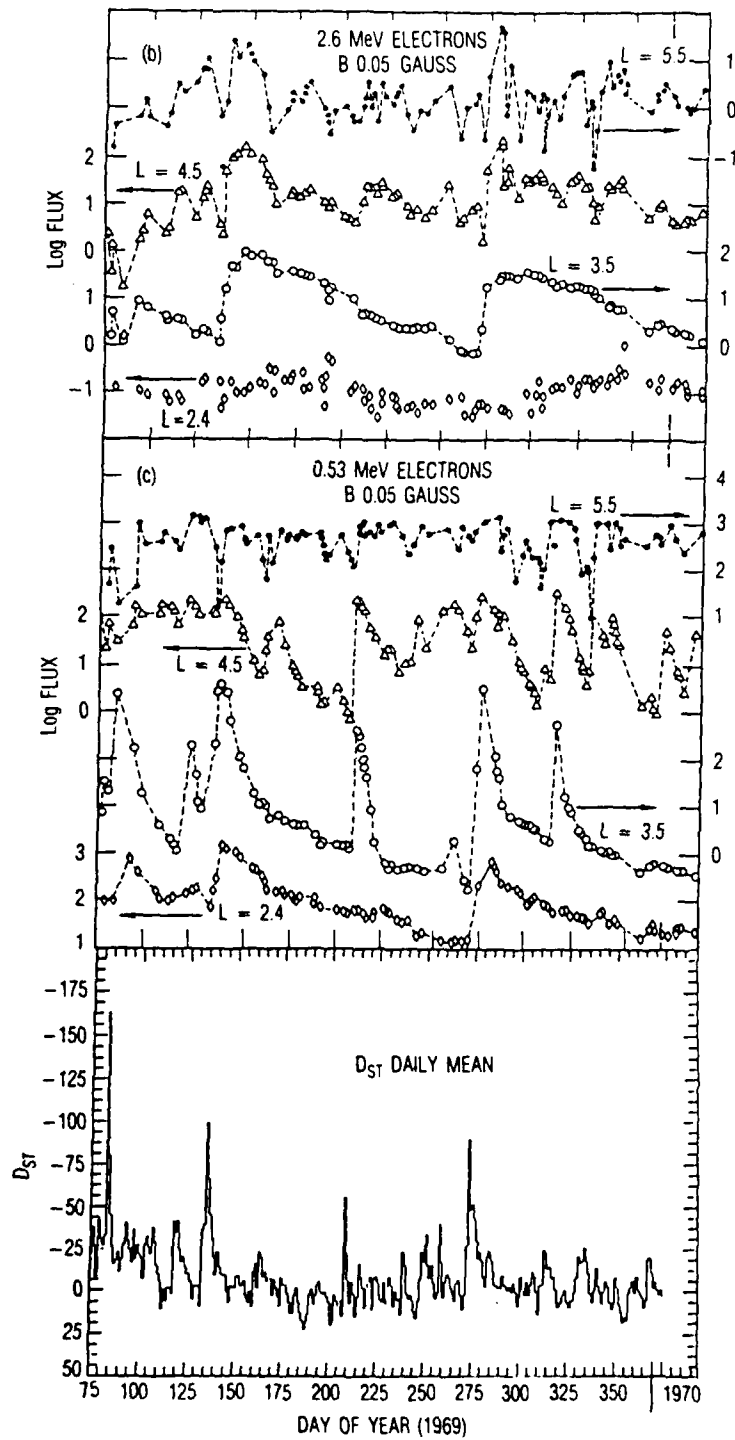Fig. 4. Magnetic Storm-Induced Electron Flux Increases

Fig. 5. Comparison of D_{st} with Energetic Electron Fluxes in 1969

25

D_{st}. At the lowest L-shell, 2.4, only the largest magnetic storms (as evidenced by large excursions in D_{st}) have a major effect on the 0.5 MeV electron population. The upper panel shows that the 2.5 MeV electron averages respond primarily to the large storms. Note that both energy ranges show great variability at L=5.5. We will return to this effect later. The general trend is: the lower the L-shell or the higher the energy, the larger the magnetic storm that is required to produce a significant effect.

Figure 5 demonstrates that there is no simple linear relationship between D_{st} and energetic electron fluxes. The largest negative value of D_{st}, at about Day 85, produced relatively minor effects, compared to the smaller D_{st} events at about Days 135 and 275. One thing to note, however, is that the latter two D_{st} events were of longer duration. Also, at about Day 320, a long duration D_{st} event, though relatively small, also produced sizable effects in the 0.5 MeV flux at L=3.5.

V. EFFECTS OF MAGNETIC ACTIVITY ON ENERGETIC PARTICLES

Having demonstrated the correlation between the sunspot cycle and D_{st} and, in turn, the correlation between D_{st} and the outer zone energetic electron population, we will now discuss the effect of the solar cycle on each of the various particle species and magnetospheric locations. At high altitudes, the major solar-activity effects which affect spacecraft, through increases in the energetic particle population, are surface and thick-dielectric charging, sensor backgrounds, heating, and radiation dose. We will consider these, in turn, making estimates of the effect of the solar cycle on each of them.

A. OUTER ZONE ELECTRONS

The outer zone electrons originate either as solar wind electrons in the tail of the magnetosphere or as ionospheric electrons at high latitudes which are accelerated up the field lines. Magnetic field fluctuations cause the outer zone electrons to be diffused radially inward, energizing them. The acceleration is a consequence of the conservation of the first adiabatic invariant coupled with violation of the third invariant, discussed earlier, by magnetic activity. As the particles are transported to field lines deeper in the magnetosphere, the increase in the average field intensity has to be compensated by an equivalent increase in particle momentum, or energy. The various fluxes peak at different locations in the outer zone for different energies, with the higher energies peaking at lower L. Representative outer zone fluxes are of the order of: $> 10^8$ for $E_e > 0.1$ MeV, L = 6; $> 10^7$ for $E_e > 1$ MeV, L = 5; $> 10^5$ for $E_e > 4$ MeV, L=4. Units are integral, omnidirectional electrons $cm^{-2}-sec^{-1}$.

Outer zone electron fluxes are highly variable, with increases caused by major magnetic storms at a given energy on a given L-shell being as great as 5 orders of magnitude in less than a day. Typical decay constants for outer zone electrons are of the order of 10 days. In addition to producing radial diffusion of the particles, magnetic storms also cause pitch-angle scattering of the particles. Thus, particles which were previously stably trapped on a field line (had mirror points that were above the atmosphere everywhere along their drift paths) can be perturbed so that they now mirror within the residual atmosphere below 100 km at some point along their drift path. At this altitude, the atmosphere absorbs the particles. A low altitude satellite which is normally below the trapped radiation zones (except when traversing the South Atlantic Anomaly) may suddenly find itself bathed in large fluxes of energetic electrons at midlatitudes when it encounters these particles, which show up low on the outer zone field lines (sometimes called the *horns* of the outer zone). The South Atlantic Anomaly is a region of anomalously low magnetic field strength.

27

Since particles mirror at a constant B_m, they attain their lowest mirror altitude in the South Atlantic Anomaly.

B. HIGH ALTITUDE SPACECRAFT SURFACE CHARGING

For high altitude spacecraft operations, spacecraft charging, radiation damage, and energetic particle backgrounds are the major areas of concern which involve environmental factors which are related to magnetic field activity. Spacecraft charging problems can originate in two different mechanisms, both of which are ultimately caused by magnetic field activity. The first mechanism is surface charging. In this process, a hot plasma causes surfaces of spacecraft to charge to high levels, sometimes to many kilovolts; discharging of differentially charged surfaces then produces spurious operation of, or damage to, the spacecraft.

An object placed in a plasma will charge negatively due to the greater mobility of the electrons as compared to the ions. One of the components in the charge-balance equation is the secondary emission from the surface due to the impacting primary. At low energies, the secondary emission ratio usually exceeds unity. At higher incident energies, typically around 1 to 2 keV, this ratio drops below unity. If the flux of electrons that arrive at the surface is primarily composed of particles with energies above this value, the surface can begin to charge. Note that the surface, once it begins to charge, prevents low energy electrons which might assist in discharging it from reaching it. As the object charges, a sheath region is created around the object which repulses the particles of like charge and attracts the opposite charge (*e.g.*, protons). Equilibrium is reached when the sheath has grown to a sufficient extent that the currents due to the plasma species are balanced. Sunlight modifies the picture in that the photocurrent from a surface is usually orders of magnitude greater than plasma currents; thus, equilibrium in sunlight is normally controlled by emission and reattraction of photoelectrons. For some configurations of surface structure, charged elements may control currents to and from nearby elements just as a grid in an electron tube does. Equilibrium for those elements, then, is determined by the satellite geometry and may be far different from what would be observed for the elements if they were placed elsewhere on the spacecraft.

For satellites in the earth's umbra and for shadowed surfaces on satellites, photoemission control of equilibrium is not available. However, at low and intermediate altitudes (up to the location of the plasmapause, which is usually found at 15,000 to 25,000 km altitude at the equator), the density of cold plasma (which has a temperature of a few eV) is high enough (10^2-10^6 cm^{-3}) that sheaths produced at small potentials are sufficient to maintain current equilibrium to surfaces. At high altitudes, such as the geosynchronous orbit region, the cold plasma density is

usually small, of the order of 1 cm^{-3}. Under some magnetic conditions, the density may drop another order of magnitude.

When the cold plasma density is low, the possibility exists that surfaces can charge to very high potentials. The source of the charging current is a high temperature plasma generated in the geomagnetic tail by substorm activity and transported to lower altitudes. The high mobility of the electrons compared to the ions (the result of the large difference in particle mass) may cause surfaces to charge to kilovolt or tens of kilovolt levels.[12] In umbra, potentials greater than 19 kV have been observed.[13] The charging of spacecraft surfaces may produce electrostatic barriers which prevent the neutralization of the spacecraft as a whole. This, then, may result in several hundred volt potentials on spacecraft in sunlight. Shadowed surfaces which charge to kilovolt levels may discharge to a spacecraft structure which has been maintained at low levels by photoelectron emission. These discharges, which may involve significant capacitance, may couple to signal leads, producing spurious operation of the spacecraft. In extreme cases, the discharges may damage components. Surface charging has been a major problem on many satellites at geosynchronous orbit.

Figure 6 shows discharges associated with a surface charging event on the P78-2 (SCATHA) spacecraft[14] while it was in the midnight sector. The upper two panels are spectrograms of the electron and ion fluxes. Lighter areas indicate higher fluxes. These spectrograms show a hot plasma injection from the tail. The average electron energy exceeded 20 keV in this event (which is sufficiently high to consider it an energetic particle event, placing it within the purview of this presentation). The magnetosphere was quite disturbed: during this period, K_p was 5$^-$ and had been 6$^-$ during the previous 3-hr period. The lowest panel shows the potential between the spacecraft structure and a Kapton sample on the surface of the vehicle. The difference in potential is due to the shadowed Kapton sample being charged by the high temperature plasma while the structure is clamped by sunlight-induced photoemission and secondary emission. The spacecraft enters eclipse at about 23.8 hr Magnetic Local Time (MLT). Just prior to this time, it is enveloped in a hot plasma. The average energy of the electrons, top panel, rises from about 1 keV to about 8 keV. The timing of the eclipse passage with the influx of hot plasma is coincidental. An electrical discharge is observed on the vehicle just as the potential is changing at its maximum rate (lowest panel). The satellite frame potential exceeded 10 kV during the eclipse. Upon exiting the hot plasma, there is again a discharge during the maximum rate of change of the vehicle frame potential with respect to the potential on the Kapton. In the case of the P78-2 satellite, these discharges did not affect the operation of the vehicle, since the vehicle was designed as a Faraday cage in an effort to study such discharges without being affected by them. However, such discharges on other satellites do have serious effects.
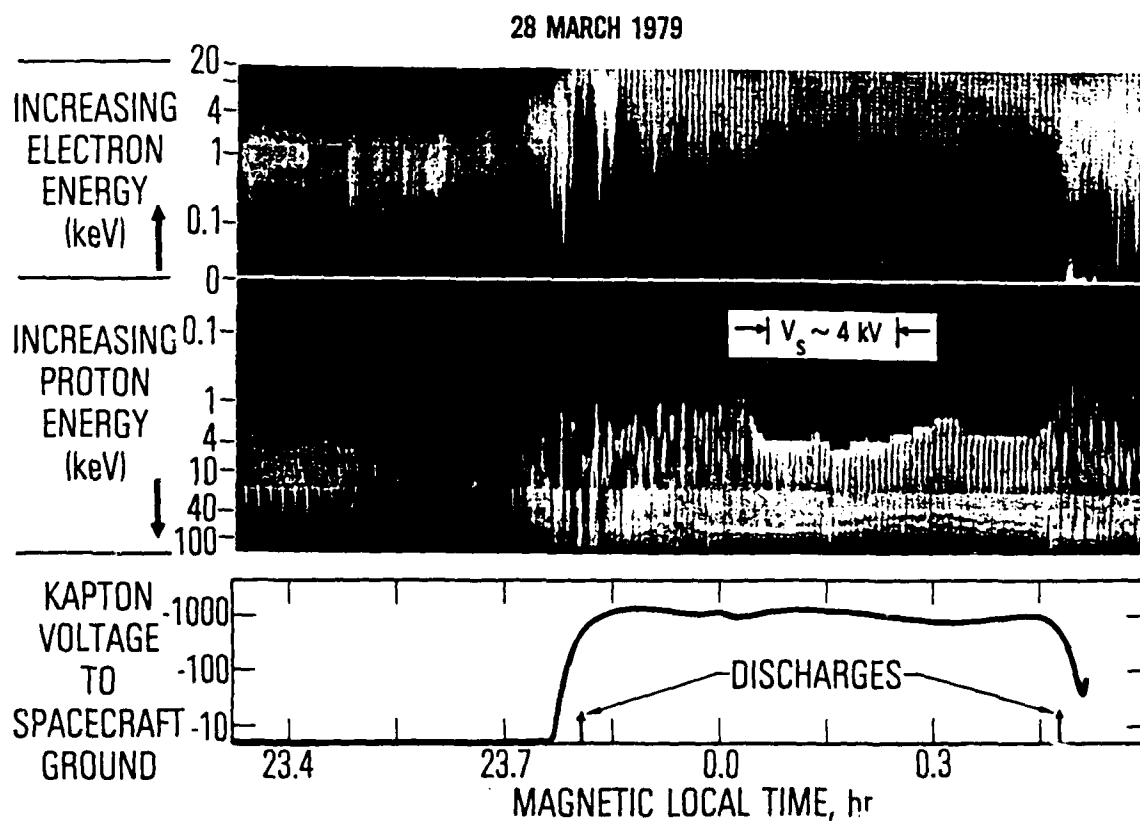
29

28 MARCH 1979

Fig. 6. Natural Charging Event on the P78-2 (SCATHA) Spacecraft in Eclipse

Surface charging is intimately connected with magnetic field activity. Figure 7 demonstrates that both the probability of charging and the maximum potential attained are related to the level of magnetic activity.[15] Figure 7 presents histograms of the probabilities of charging versus MLT observed by the SCATHA Satellite Surface Potential Monitor (SSPM) on two Kapton samples.[15] The voltage indicated is the potential with respect to the spacecraft frame. Figure 7a is the histogram of charging probabilities during magnetically quiet times ($K_p < 2^+$), and Fig. 7b is a similar plot for probabilities during more disturbed periods ($K_p > 2^+$). Note that the level of magnetic activity has a large effect on both the probability of charging and the degree of charging. Thus, increased geomagnetic activity which would result from a more robust solar cycle would also result in increased frequency and severity of surface charging events on satellites in the outer magnetosphere. It is difficult to make a direct quantitative estimate of these increases, even if we knew what the solar cycle will be, because the MLT of the satellite at the time of a hot plasma injection determines what the effect will be. The correlation between the aa index[5] (a 3-hourly global magnetic index generated with data from two antipodal stations) and the sunspot number indicates that, on the average, hot plasma injections should be about twice as prevalent in the coming solar cycle as in the past one.

C. HIGH ALTITUDE THICK DIELECTRIC CHARGING

At geosynchronous altitude, the more energetic electron population ($E_e > 40$ keV) is usually near the Kennel-Petschek[16] limit. (Above the Kennel-Petschek limit, a wave-particle instability causes pitch-angle scattering of the particles, with the result that some particles are lost into the atmosphere. The flux density is thus self-limiting.) The effect of moderate magnetic storms is to temporarily depopulate these field lines of energetic electrons (a flux *dropout*), but they are refilled almost immediately. Since small magnetic storms are equally effective, there is no significant solar-cycle dependency in the average geosynchronous orbit electron fluxes. Major storms, however, produce large fluxes of very energetic electrons deeper in the magnetosphere, L~3.5 to 4, which then diffuse back out, producing a harder spectrum (more electrons with $E_e > 1$ MeV). The lower trace in Fig. 8 is a plot of the $E_e > 1.2$ MeV electron flux as measured at geosynchronous orbit by the GOES weather satellites from mid-1980 to mid-1982. The arrows indicate times when sun-sensor anomalies ascribed to thick dielectric charging were experienced on several geosynchronous satellites.[3] The upper panel is a plot of D_{st} for the same time period. Again, while there is a strong correlation between the $E_e > 1.2$ MeV electron flux and D_{st}, there is no unique linear relationship. However, there is a systematic delay of 1 to 2 days between the peak in D_{st} and the increase in the energetic electrons. This delay is interpreted as being the time required for electrons to diffuse out to geosynchronous orbit from the heart of the outer zone where they are accelerated by the magnetic storms. The lack of a perfect correlation between the

31

SSPM
PROBABILITIES OF CHARGING

QUIET
$(K_p \leq 2_+)$

> 100 Volts
> 500 Volts

KAPTON-2　　　　　　KAPTON-1

L > 6.6 Re

L ≤ 6.6 Re

MLT (hr)

SSPM
PROBABILITIES OF CHARGING

DISTURBED
$(K_p > 2_+)$

> 100 Volts
> 500 Volts

KAPTON-2　　　　　　KAPTON-1

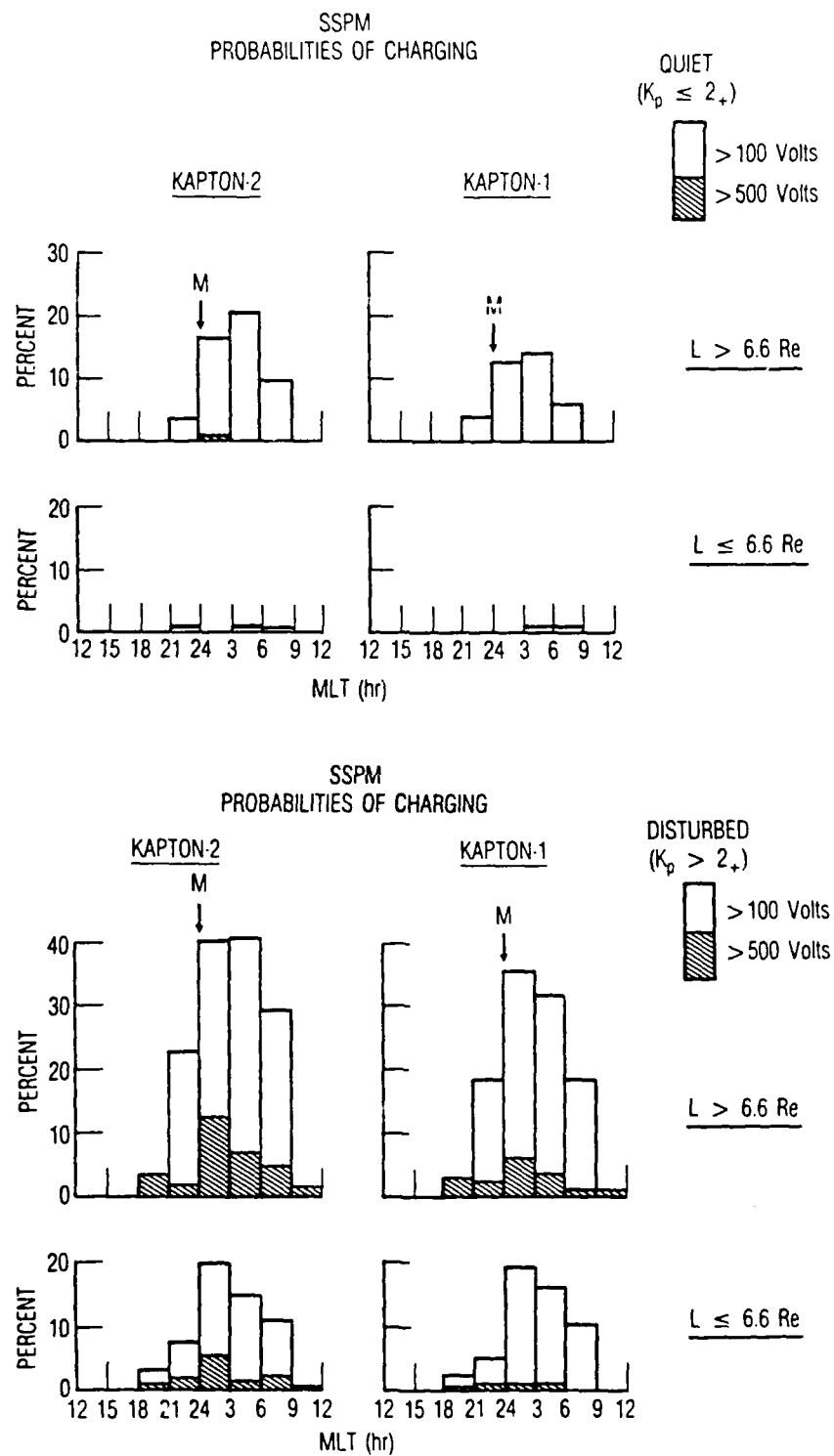L > 6.6 Re

L ≤ 6.6 Re

MLT (hr)

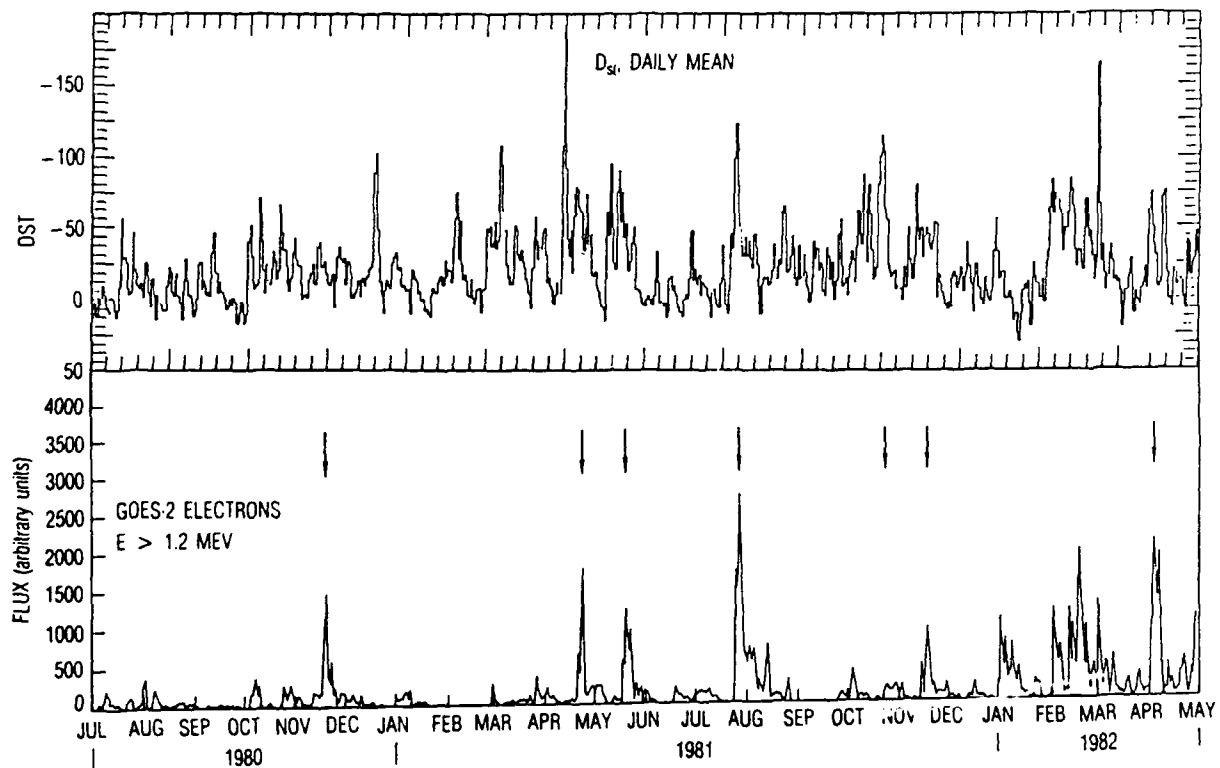Fig. 7. Histograms of the Probabilities of Charging versus Magnetic Activity

32

Fig. 8. Comparison of D_{st} with Energetic Electrons Measured by GOES

anomalies and the electron flux was interpreted as being the result of measuring only the >1.2 MeV electrons, while it is the 0.5 to 1.0 Mev electrons that are primarily responsible for thick dielectric charging.

Since magnetic activity has a major effect at geosynchronous orbit only on the very energetic electrons ($E_e \geq 2$ MeV), the effect of a robust solar cycle on satellites in that region should be modest. In addition to the increased probability of surface charging described above, one could also expect an increased occurrence of energetic electron infusions. These would result in a higher frequency of occurrence of thick dielectric discharges (on those satellites that are subject to them) and an increased frequency of background contamination in heavily shielded sensors. The net effect on the radiation dose and particle-induced heating should be less than the uncertainty limits in any prediction of these effects using the standard environmental models. At this time, the present solar cycle, Cycle 22, appears to be similar to Cycle 19. Basing an estimate of the frequency of occurrence of major storms on Cycle 19 produces a prediction that the frequency of thick dielectric charging anomalies will be about a factor of 2 higher than nominal.

D. OUTER ZONE ENERGETIC ELECTRON VARIABILITY

As has been shown previously (Figs. 4 and 5), major magnetic storms have a major effect on the energetic electron environment in the heart of the outer zone. Virtually all of the energetic flux observed in the outer zone results from moderate ($D_{st} < -50$ nanotesla) to major ($D_{st} < -150$ nanotesla) magnetic storms. Between storms, the electron flux decays away monotonically. The NASA models are averaged over the solar cycle. A long-term mission at L=3.5 would experience about 50% of the total fluence in about 3% of the time, 70% of the fluence in 10% of the time, and 80% of the fluence in 30% of the time.

In the outer zone, there is a large difference between solar minimum and solar maximum as far as the energetic electrons are concerned, even though the solar MIN and MAX versions of the AE8 electron model differ only in their inner zone fluxes.[17] We will address the models in detail in the next section. From the point of view of major energetic electron increases during Cycle 20, there was an average of one major and one moderate storm per year. However, the distribution was quite skewed. During solar minimum, only one storm per year occurred, on average, while during the peak (and the year or two thereafter), the annual average was three storms. Thus a 2- or 3-year mission would see three times as many storms near solar maximum as at solar minimum. Again using Cycle 19 as a standard, one would predict that the peak in magnetic activity during Cycle 22 would produce about six major or moderate storms per year. While this is only a factor of 2 above that observed in Cycle 20, it is a factor of 3 higher than the NASA environmental models. Added to this is the concern that the NASA models understate the

very energetic electron flux ($E_e > 2$ MeV) in the outer zone.[18,19] The result is that effects due to energetic electrons in the outer zone (such as radiation dose, heating, thick dielectric charging, and sensor backgrounds) may be a factor of 4 or 5 more severe than the models predict.

E. OUTER ZONE PROTONS

Magnetic activity has relatively little effect on the outer zone protons. The primary effect after a major storm is an increase in the number of low energy ($E_p < 300$ keV) protons. Above this energy, only short-term (1 to 2 days) flux changes of 1/2 to 1 order of magnitude are observed. The lower energy proton flux changes are also short term (as evidenced by the D_{st} recoveries, which are the signature of the low energy proton ring current injected by the storm), but intensity changes can be 1 to 2 orders of magnitude. For satellite systems, these changes are of concern only from the point of view of peak thermal input to low temperature radiators. Compared to the effects on the electrons, the effect of an enhanced solar cycle on the outer zone protons would be very benign.

F. INNER ZONE ELECTRONS

The source of the inner zone electrons is a combination of cosmic-ray albedo neutron decay (CRAND) and radial diffusion through the slot from the outer zone. In the CRAND mechanism, cosmic rays interact with air molecules in the upper atmosphere, producing energetic neutrons, some of which escape back into space. Since neutrons are uncharged, they cross magnetic field lines unimpeded. However, some neutrons decay while still in the magnetosphere, and the decay products, an electron and a proton, are charged and so become trapped. The end-point energy of the electron in neutron decay is slightly under 1 MeV. The contribution of the neutron's velocity to the electron's energy is small. As a result, there are few electrons with energies in excess of 1 MeV in the inner zone. Electrons with higher energies are present in small numbers, especially above about L=1.65 after large magnetic storms, but can be ignored as a hazard to space systems except for their background effects in sensors.

Inner zone electrons below about 1000 km have lifetimes that are primarily determined by the scale height of the atmosphere. During solar-active periods, the increased scale height results in a reduced lifetime and lower average fluxes. This is reflected in the NASA AE8 and AP8[20] models by having a solar maximum and a solar minimum version. Farther out in the inner zone, electrons are quite stable, with typical lifetimes of 400 days.[21] Principal loss mechanisms are probably any or all of the following: radial diffusion into the atmosphere (violation of the second and third invariants caused by magnetic storms); interaction with whistler-mode waves produced

by lightning strokes (the resonant interaction between these waves, also known as cyclotron waves, and the electrons results in a lowering of the electron pitch angle, causing it to be absorbed by the atmosphere at the end of the field line); and interaction with VLF waves from ground-based transmitters, which similarly lowers pitch angles.

The order of magnitude of the electron fluxes at L=1.45 in the inner zone is as follows: > 10^8 for $E_e > 0.1$ MeV; > 10^6 for $E_e > 1$ MeV; > 10^5 for $E_e > 2$ MeV. The numbers represent the integral, omnidirectional fluxes cm^{-2}-sec^{-1}. Below about L = 1.55, the fluxes are quite stable, with little variation being observed over the solar cycle[22] except for altitudes below 1000 km where atmospheric effects are observed. Above L= 1.6, major magnetic storms inject electrons with energies up to at least 1.2 MeV.[9]

G. LOW ALTITUDES

For low altitude spacecraft, surface charging is not, in general, a significant problem. Because of the high density of the cold plasma, relatively low potentials (a few tens of volts) are sufficient to ensure current balance. There are scenarios in which this may not be the case (a surface in the wake of a very large object traversing the auroral zone, for example), but they are rare. Similarly, variations in energetic particle fluxes due to magnetic activity are not normally a major concern, because low altitude spacecraft with low orbital inclinations spend all of their time in the inner zone where flux perturbations are small. Figure 9 is a plot[23] of inner zone low energy electrons (E_e>0.28 MeV) for L=1.2, 1.3, 1.5, 1.8, and 2.2 for the time period 1963 to 1969. The response of these fluxes to magnetic activity is pronounced. The lower plot is the daily mean D_{st}. Figure 9 shows that no magnetic storms, even those with D_{st}<-300 nanotesla, increased inner zone fluxes by more than an order of magnitude. (The overall monotonic decay of flux intensity is the result of the decay of the Starfish[24] electrons which were injected in July 1962.) At L=2.2, which is in the slot region, large transient increases are seen, similar to the increases seen in the 0.5 MeV fluxes in Fig. 5 at L=2.4.

At high inclination, a low altitude satellite may traverse the auroral zones and the polar cap. In these regions, two effects may be of importance to missions: (a) the geomagnetic control of entry of solar and galactic cosmic rays; (b) auroral precipitations. Cosmic rays may constitute either an undesired background in sensors or an enhanced probability of circuit malfunction (due to the SEU--Single Event Upset--a phenomenon caused by a direct creation of electron/ion pairs within a solid-state circuit by a highly ionizing particle which changes the state of the circuit, sometimes destructively). Magnetic activity, of course, changes the cutoff latitude for entry of cosmic rays and thus the probability of SEU events as a function of latitude. These topics also are beyond the scope of this presentation and will not be discussed further.
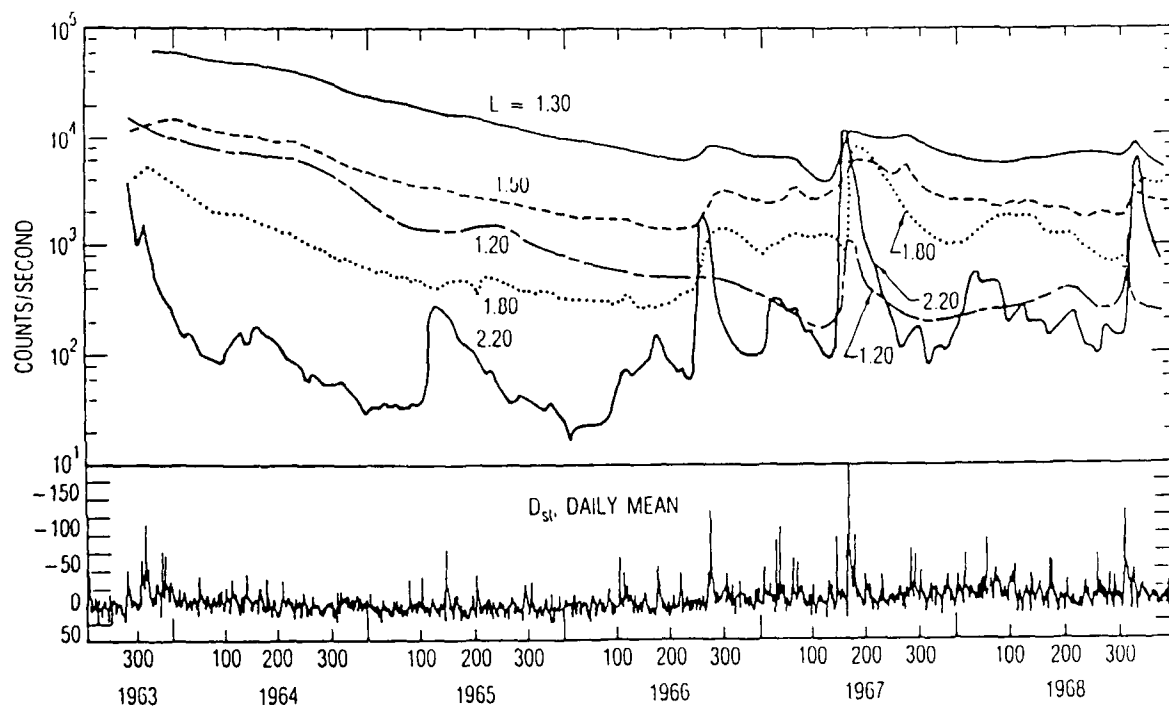
Fig. 9. Inner Zone Electron Fluxes for 1964 to 1968

The Sub Auroral Red (SAR) arc is another energetic particle phenomenon with a relationship to magnetic activity which may affect spacecraft missions. In this mechanism, lower energy (>20 keV) protons from the ring current produced by magnetic storms precipitate into the atmosphere and produce kilo-Rayleigh light intensities at intermediate latitudes, typically around 55°-65° magnetic latitude.[25] Accompanying the proton precipitation is relativistic electron precipitation in the same region.[26,27] The electron and proton energy is degraded via Landau damping. The interaction with the atmosphere produces a diffuse red area which may interfere with optical systems on low altitude satellites. Production of a SAR arc usually requires a major magnetic storm. To the extent that major storms may be more prevalent during Cycle 22, one can expect perhaps a doubling in the numbers of SAR arcs and more frequent arcs at low latitude. (The larger the storm, the lower the latitude at which the SAR arcs occur.)

H. INNER ZONE ENERGETIC PROTONS

The source of the energetic protons which are present in the inner zone is CRAND, the mechanism mentioned previously. The energetic protons are quite stable, with minor variations in intensity occurring at low altitudes due to variations in the atmospheric density resulting from solar activity. Typical intensities at $L = 1.45$ are of the order of: $> 10^4$ for $E_p > 100$ MeV and $> 10^3$ for $E_p > 300$ MeV. These are omnidirectional, integral fluxes in units of cm^{-2}-sec^{-1}. The current model, AP8, has a MIN and a MAX version, relating to solar minimum and solar maximum. The solar maximum version has lower proton fluxes. The increased solar activity results in an increased atmospheric scale height which, in turn, results in an increased removal rate of energetic particles at the lower L-values. The effect is small.

I. LOW ENERGY PROTONS

The low energy protons with which we are concerned here are in the 0.5-5 MeV range, since there are large fluxes of such particles in both the inner and outer zone and the protons have significant materials and thermal effects. Particles with these energies can originate in a number of sources: radial diffusion and energization of solar wind particles which enter the geomagnetic tail, similar to the outer zone electrons; ionospheric acceleration up field lines, with subsequent radial diffusion and acceleration; and direct access of solar flare protons. Typical intensities in the outer zone are: $> 10^8$ for $Ep > 0.1$ MeV; $> 10^7$ for $Ep > 1$ MeV; $> 10^5$ for $Ep > 10$ MeV; $< 10^2$ for $E_p > 100$ MeV. Again, these are omnidirectional, integral fluxes in units of cm^{-2}-sec^{-1}. While the fluxes are subject to variation due to magnetic storm activity, the variations are much smaller than for electrons. The primary loss mechanisms are deenergization through collisions with the

residual atmosphere, and charge exchange, which results in an energetic neutral particle which is not trapped by the magnetic field. The comments made previously about the solar cycle effects on outer zone protons also apply here.

VI. USE OF PARTICLE MODELS DURING CYCLE 22

Since various particle models are used in the design of spacecraft, subsystems, and in mission planning, it is useful to address the probable effect of a robust Cycle 22 on their accuracy. We shall discuss the models by the location of application, since the solar cycle effects are different in the different parts of the magnetosphere.

A. INNER ZONE ELECTRON MODELS

The current NSSDC models which provide useful inner zone (L = 1.2 to 2.4) electron data are AE5,[22] for solar minimum; AE6,[28] for solar maximum; and AE8, for either solar minimum or solar maximum. The energy range of these models is from 0.04 to 5 MeV, although present techniques cannot make reliable measurements of electrons with energies above 2 MeV below about L=1.55 in the inner zone. These are empirical models, being based on in-situ measurements of the fluxes made between 1964 and 1968. Note that that time period was during the rising part of Cycle 20, which was the smallest of the last six solar sunspot cycles. The solar cycle influences on electrons in the inner zone are limited to the effect of an increased atmospheric scale height (which reduces the electron flux at altitudes below 1000 km) and an increased diffusion rate of electrons through the slot region. This second effect is noticeable in the vicinity of L=1.65-1.75 at energies above 1 MeV for a short period after major magnetic storms. The effect of either of these processes is small and can be ignored in comparison to the normal environment. Cycle 22 is not a concern here.

B. OUTER ZONE ELECTRON MODELS

The current NSSDC outer zone models (L > 2.4) which provide useful results are the following: AE7-Lo and AE8 for solar minimum and AE7-Hi for solar maximum or long duration missions (> 5 years). For geosynchronous satellites, another model is still relatively valid-- AE3.[29] For long-term missions, AE7-Hi is probably accurate to within a factor of 2, especially for L < 6 and E < 5 MeV. This model was generated from data obtained during 1969, the peak of Cycle 20. The data were corrected and averaged for a complete cycle. However, if a mission includes the period a year or two following the sunspot maximum, when the magnetic storm activity is greatest, AE7-Hi will err on the low side (actual integrated fluences can be expected to be greater than the model prediction). AE7-Hi was generated in response to criticisms that the earlier models, AE4 and AE6, were seriously deficient in high energy electrons. In fact, in those

models, the energy spectra were truncated at 5 MeV, which is also done in AE8. A comparison of the models with in-situ data[9] showed that the models predicted fluxes that were low by about a factor of 3, but almost the entire deficiency was in electrons > 1.5 MeV. The result was a prediction of dose in heavily shielded satellite components that was low by an order of magnitude. AE7-Hi, which truncates the energy spectrum at 7.5 MeV, has also been criticized for truncating the spectrum, since electrons with energies up to 10 MeV have been measured at geosynchronous orbit.[18]

AE8 exists in two forms, AE8MIN and AE8MAX, which are supposed to represent the environment during solar minimum and maximum. However, both forms are truncated at 5 MeV and cannot properly model the solar maximum period, when large fluxes of very energetic electrons appear. AE8 uses a single outer zone model and uses AE5 and AE6 solar minimum and solar maximum inner zone models. The major difference between AE8 and AE7-Hi is in the high energy electron flux at around L = 4. The AE7-Hi model contains about a factor of 2 greater flux at 3 MeV and about a factor of 10 greater flux at 4.5 MeV. At solar minimum, there are relatively few energetic electrons and any of the later models--AE7-Hi, AE7-Lo, AE8MIN, and AE8MAX-- are satisfactory for any use except for calculating background rates in detectors. The models are probably accurate to a factor of 3 for dose calculations. For a projected Cycle 22 that is equivalent to Cycle 19, AE7-Hi would probably be an additional factor of 2 low (over and above the factors mentioned in the preceding paragraph). AE8-MAX would grossly underestimate the electron flux above 1.5 MeV.

C. PROTON MODELS

The current proton models are AP8MIN and AP8MAX, again representing the solar minimum and maximum periods. The major effect of the solar variation is the variation in atmospheric density at lower altitudes. The models are probably accurate to 50% or better. They cover the energy range from 100 keV to 400 MeV and the L range from 1.17 to 7. The data were obtained during the same time period that the inner zone electron data were obtained. Since the MIN model predicts slightly more flu · than the MAX model, it can be used during solar maximum or for long-term missions as a conservative model. A robust Cycle 22 should not produce major errors in estimates of fluxes.

One major area which has not been modeled is the dynamics of the radiation belts in response to magnetic activity. One report[30] attempts to correlate the response of the outer zone electrons to the magnetic index K_p, but the particle data were all obtained at geosynchronous orbit, and the field lines that are represented in the K_p index are high latitude field lines which thread through the geosynchronous region. Hence, that study is limited in validity to the

geosynchronous region. Low altitude measurements indicate that, in general, the outer zone does not correlate with K_p, except incidentally when major magnetic storms occur, but does have some relationship with D_{st}.

VII. SUMMARY

The preceding and following conclusions are the opinions of the author; they have not been discussed with other magnetospheric particle researchers and thus are not a consensus. With that warning, we will proceed to make some predictions. If Cycle 22 is similar to Cycle 19, the general trend among the various particle populations and environmental effects on satellites should be the following.

1. Any additional effects (over and above the normal solar cycle effects) on energetic inner zone protons and inner zone electrons below L=1.6 can be ignored.

2. Noticeable effects on inner zone electrons will be limited to energies above 1 MeV at L>1.6.

3. Outer zone protons, especially the ring current, will on average be elevated due to an expected higher frequency of large magnetic storms. Satellites in the outer zone which use cryogenic radiators will be subject to more frequent increases in heat input.

4. Surface charging in the near-synchronous orbit region can be expected to be more frequent and more severe. The same is true of thick dielectric charging.

5. The outer zone energetic electron environment can be expected to be much more severe than has been previously observed. The models will seriously underestimate the $E_e > 1.5$ Mev fluxes: AE7-Hi by perhaps a factor of 4 and AE8MAX by an order of magnitude.

REFERENCES

1. A. L. Vampola, J. E. Cox, and R. D. Jiminez, "Heat Loads due to the Space Particle Environment," *J. Spacecraft and Rockets* (in press).

2. A. Meulenberg, Jr., "Evidence for a new Discharge Mechanism for Dielectrics in Plasma," in *Spacecraft Charging by Magnetospheric Plasmas*, AIAA Progress Series, *Vol. 47*, A. Rosen, ed. (1976), pp. 236-247.

3. A. L. Vampola, "Thick Dielectric Charging on High-Altitude Spacecraft," *J. Electrostatics 20*, 21 (1987); also in *The Aerospace Environment at High Altitudes and its Implications for Spacecraft Charging and Communications, AGARD CP 406* (1986) p. 28-1.

4. D. A. McPherson and W. R. Schober, "Spacecraft Charging at High Altitudes: The SCATHA Satellite Program," in *Spacecraft Charging by Magnetospheric Plasmas*, AIAA Progress Series, *Vol. 47*, A. Rosen, ed. (1976) pp. 15-30.

5. D. J. Gorney, "Solar Cycle Effects on Near-Earth Plasmas and Space Systems," *J. Spacecraft and Rockets* (in press).

6. G.L. Withbroe, "The Solar Activity Cycle: History and Predictions," *J. Spacecraft and Rockets* (in press).

7. M. Schulz and L. J. Lanzerotti, *Particle Diffusion in the Radiation Belts*, Springer-Verlag, New York (1974).

8. C. E. McIlwain, "Coordinates for Mapping the Distribution of Magnetically Trapped Particles," *J. Geophys. Res. 66*, 3681 (1961).

9. A. L. Vampola, "Natural Variations in the Geomagnetically Trapped Electron Population," in *Proceedings of the National Symposium on Natural and Manmade Radiation in Space*, NASA TM X-2440, E. A. Warman, ed. (1972), pp. 539-547.

10. A. L. Vampola, J. B. Blake, and G. A. Paulikas, "A New Study of the Magnetospheric Electron Environment," *J. Spacecraft and Rockets 14*, 690 (1977).

11. D. J. Williams, J. F. Arens, and L. J. Lanzerotti, "Observations of Trapped Electrons at Low and High Altitude," *J. Geophys. Res. 73*, 5673 (1968).

12. S. E. Deforest, "Spacecraft Charging at Synchronous Orbits," *J. Geophys. Res. 77*, 651 (1972).

13. R. C. Olsen, "The Record Charging Events from ATS6," *J. Spacecraft and Rockets 24*, 362 (1987).

14. H. C. Koons, "Summary of Environmentally-Induced Electrical Discharges on the P78-2 (SCATHA) Satellite," *J. Spacecraft and Rockets 20*, 425 (1983).

15. P. F. Mizera, "A Summary of Spacecraft Charging Results," *J. Spacecraft and Rockets 20*, 438 (1983).

16. C. F. Kennel and H. E. Petschek, "Limit on Stably Trapped Particle Fluxes," *J. Geophys. Res. 71*, 1 (1966).

17. A. L. Vampola, Chairman, "Trapped Radiation Effects Panel Report," in *NASA/SDIO Space Environmental Effects on Materials Workshop* , NASA Conference Publication 3035, Pt. 2, Hampton, Virginia, June 1988, B. A. Stein and L. A. Teichman, eds. (1989), pp. 597-605.

18. D. N. Baker, R. D. Belian, P. R. Higbie, R. W. Klebesadel, and J. B. Blake, "Hostile Energetic Particle Radiation Environments in Earth's Outer Magnetosphere," in *The Aerospace Environment at High Altitudes and its Implications for Spacecraft Charging and Communications, AGARD CP 406* (1986), p. 4-1.

19. A. L. Vampola, "The Space Particle Environment," in *NASA/SDIO Space Environmental Effects on Materials Workshop* , NASA Conference Publication 3035, Pt. 2, Hampton, Virginia, June 1988, B. A. Stein and L. A. Teichman, eds. (1989), pp. 367-382.

20. D. M. Sawyer and J. I. Vette, *AP-8 Trapped Proton Environment, NSSDC WDC-A-R&S 76-06* (1976).

21. E. G. Stassinopoulos and P. Verzariu, "General Formula for Decay Lifetimes of Starfish Electrons," *J. Geophys. Res. 76*, 1841 (1971).

22. M. J. Teague and J. I. Vette, *The Inner Zone Electron Model AE-5, NSSDC WDC-A-R&S 72-10* (1972).

23. C. O. Bostrom, D. S. Beall, and J. C. Armstrong, "Time History of the Inner Radiation Zone, October 1963 to December 1968," *J. Geophys. Res. 75*, 1246 (1970).

24. W. N. Hess, "Collected Papers on the Artificial Belt from the July 9, 1962 Nuclear Detonation," *J. Geophys. Res. 68*, 605 (1962).

25. J. M. Cornwall, F. V. Coroniti, and R. M. Thorne, "Unified Theory of SAR Arc Formation at the Plasmapause," *J. Geophys. Res. 76*, 4428 (1971).

26. A. L. Vampola, "Electron Pitch-Angle Scattering in the Outer Zone During Magnetically Disturbed Times," *J. Geophys. Res. 76*, 4685 (1971).

27. R. M. Thorne and C. F. Kennel, "Relativistic Electron Precipitation during Magnetic Storm Main Phase," *J. Geophys. Res. 76*, 4446 (1971).

28. M. J. Teague, K. W. Chan, and J. I. Vette, *AE-6: A Model Environment of Trapped Electrons for Solar Maximum, NSSDC WDC-A-R&S 76-04* (1976).

29. J. I. Vette and A. B. Lucero, *Models of the Trapped Radiation Environment, Vol. III: Electrons at Synchronous Altitudes, NASA SP-3024* (1967).

30. T. Nagai, "Space Weather Forecast: Prediction of Relativistic Electron Intensity at Synchronous Orbit," *Geophys. Res. Lett. 15*, 425 (1988).

NOMENCLATURE

B	local magnetic field
B_i	magnetic field intensity at location i
B_m	value of B at the mirror points
B_0	reference earth equatorial surface magnetic field
c	velocity of light
D_{st}	low-latitude geomagnetic field index, nanoteslas
E	Electric field
E_e	electron energy
E_p	proton energy
eV	electron volt
f_L	Larmor frequency
Hz	hertz
I	invariant of bounce motion
keV	kilo electron volts
km	kilometer
K_p	planetary high latitude magnetic index
L	McIlwain's parameter
M	magnetic moment
M_e	dipole moment of the geomagnetic field
MeV	mega electron volts
MHz	megahertz
MLT	magnetic local time
m	mass of particle
m_0	rest mass
$p_\perp$	momentum perpendicular to the magnetic field line
q	charge on an electron or ion
R	radial distance
R_e	Earth radius
R_0	normalized dipole radius to geomagnetic equator
UV	ultra violet light
v	velocity
VLF	very low frequency electromagnetic waves
y	$\sin \alpha$
α	equatorial pitch angle
α_i	particle pitch angle at location i
ΔB	change in magnetic field
γ	relativistic mass ratio, $= 1/(1-v^2/c^2)^{1/2}$
λ	magnetic latitude
ρ	radius of gyration
Ω_1	frequency of gyration
Ω_2	bounce frequency
Ω_3	drift frequency

LABORATORY OPERATIONS

The Aerospace Corporation functions as an "architect-engineer" for
national security projects, specializing in advanced military space systems.
Providing research support, the corporation's Laboratory Operations conducts
experimental and theoretical investigations that focus on the application of
scientific and technical advances to such systems. Vital to the success of
these investigations is the technical staff's wide-ranging expertise and its
ability to stay current with new developments. This expertise is enhanced by
a research program aimed at dealing with the many problems associated with
rapidly evolving space systems. Contributing their capabilities to the
research effort are these individual laboratories:

Aerophysics Laboratory: Launch vehicle and reentry fluid mechanics, heat
transfer and flight dynamics; chemical and electric propulsion, propellant
chemistry, chemical dynamics, environmental chemistry, trace detection;
spacecraft structural mechanics, contamination, thermal and structural
control; high temperature thermomechanics, gas kinetics and radiation; cw and
pulsed chemical and excimer laser development including chemical kinetics,
spectroscopy, optical resonators, beam control, atmospheric propagation, laser
effects and countermeasures.

Chemistry and Physics Laboratory: Atmospheric chemical reactions,
atmospheric optics, light scattering, state-specific chemical reactions and
radiative signatures of missile plumes, sensor out-of-field-of-view rejection,
applied laser spectroscopy, laser chemistry, laser optoelectronics, solar cell
physics, battery electrochemistry, space vacuum and radiation effects on
materials, lubrication and surface phenomena, thermionic emission, photo-
sensitive materials and detectors, atomic frequency standards, and
environmental chemistry.

Computer Science Laboratory: Program verification, program translation,
performance-sensitive system design, distributed architectures for spaceborne
computers, fault-tolerant computer systems, artificial intelligence, micro-
electronics applications, communication protocols, and computer security.

Electronics Research Laboratory: Microelectronics, solid-state device
physics, compound semiconductors, radiation hardening; electro-optics, quantum
electronics, solid-state lasers, optical propagation and communications;
microwave semiconductor devices, microwave/millimeter wave measurements,
diagnostics and radiometry, microwave/millimeter wave thermionic devices;
atomic time and frequency standards; antennas, rf systems, electromagnetic
propagation phenomena, space communication systems.

Materials Sciences Laboratory: Development of new materials: metals,
alloys, ceramics, polymers and their composites, and new forms of carbon; non-
destructive evaluation, component failure analysis and reliability; fracture
mechanics and stress corrosion; analysis and evaluation of materials at
cryogenic and elevated temperatures as well as in space and enemy-induced
environments.

Space Sciences Laboratory: Magnetospheric, auroral and cosmic ray
physics, wave-particle interactions, magnetospheric plasma waves; atmospheric
and ionospheric physics, density and composition of the upper atmosphere,
remote sensing using atmospheric radiation; solar physics, infrared astronomy,
infrared signature analysis; effects of solar activity, magnetic storms and
nuclear explosions on the earth's atmosphere, ionosphere and magnetosphere;
effects of electromagnetic and particulate radiations on space systems; space
instrumentation.